Optics and Lasers in Engineering 80 (2016) 45–51

Contents lists available at ScienceDirect

Optics and Lasers in Engineering

journal homepage: www.elsevier.com/locate/optlaseng

Enhanced electrical and optical properties of room temperature deposited Aluminium doped Zinc Oxide (AZO) thin films by excimer laser annealing

S.O. El hamali [a,*], W.M. Cranton [a,b], N. Kalfagiannis [a], X. Hou [c], R. Ranson [a], D.C. Koutsogeorgis [a]

[a] School of Science and Technology, Nottingham Trent University, Clifton Lane, Nottingham NG11 8NS, UK
[b] Materials and Engineering Research Institute, Sheffield Hallam University, Howard Street, Sheffield S1 1WB, UK
[c] Mechanics, Materials and Structures Research Division, Faculty of Engineering, The University of Nottingham, Nottingham NG7 2RD, UK

ARTICLE INFO

Article history:
Received 26 August 2015
Received in revised form
1 December 2015
Accepted 17 December 2015

Keywords:
Transparent conductive oxide
Al-doped zinc oxide
RF-magnetron sputtering
Excimer laser annealing

ABSTRACT

High quality transparent conductive oxides (TCOs) often require a high thermal budget fabrication process. In this study, Excimer Laser Annealing (ELA) at a wavelength of 248 nm has been explored as a processing mechanism to facilitate low thermal budget fabrication of high quality aluminium doped zinc oxide (AZO) thin films. 180 nm thick AZO films were prepared by radio frequency magnetron sputtering at room temperature on fused silica substrates. The effects of the applied RF power and the sputtering pressure on the outcome of ELA at different laser energy densities and number of pulses have been investigated. AZO films deposited with no intentional heating at 180 W, and at 2 mTorr of 0.2% oxygen in argon were selected as the optimum as-deposited films in this work, with a resistivity of 1×10^{-3} Ω.cm, and an average visible transmission of 85%. ELA was found to result in noticeably reduced resistivity of 5×10^{-4} Ω.cm, and enhancing the average visible transmission to 90% when AZO is processed with 5 pulses at 125 mJ/cm^2. Therefore, the combination of RF magnetron sputtering and ELA, both low thermal budget and scalable techniques, can provide a viable fabrication route of high quality AZO films for use as transparent electrodes.

1. Introduction

Transparent conducting oxides (TCOs) are ubiquitous in a wide range of optoelectronic devices such as flat panel displays, thin film solar cells, and transparent thin film transistors [1–3]. Amongst the TCOs family, tin-doped indium oxide (ITO) has been the material of choice for transparent electrode applications. However, although ITO exhibits superior conductivity and transparency with less thickness-dependent resistivity, there is a general desire in the sector to move towards an alternative solution for advanced application of TCOs [2–4]. For instance, flexible applications that impose additional fabrication and environmental constraints such as low thermal budget fabrication and electrical conductivity stability against stretching and bending forces to which ITO is not ideally applicable [3,5]. TCO research has been directed towards exploring reduced indium content or even non-indium based transparent conducting materials such as ZnO-based transparent electrodes. ZnO has been extensively explored for various opto-electronic fields because of its attractive characteristics including, but not limited to, high exciton binding energy of 60 meV, wide and direct band gap of 3.37 eV, low growth temperature as a crystalline material, and high thermal and chemical stability. Furthermore, the ZnO characteristics can be tuned via doping in order to meet various applications requirements. For instance, doping with MgO or CdO results in larger or smaller band gap respectively [6–8]. While, doping with group III elements (Al, Ga and In) results in high quality transparent electrodes. In particular aluminium doped zinc oxide (AZO), due to its low raw material cost and comparable electrical and optical properties to ITO [2,3,8], has attracted much attention for replacing ITO in mass production of photovoltaic devices [1]. AZO was also successfully applied to organic light emitting diodes [9], and to liquid crystal displays [10].

There has been a large body of reported investigations into the fabrication of AZO via various vacuum and solution based deposition techniques such as magnetron sputtering [11–13], pulsed laser deposition [14,15], atomic layer deposition [9], sol–gel process [16], chemical vapour deposition [17], and aqueous

* Corresponding author. Tel.: +44 115 848 83163.
E-mail address: N0231027@ntu.ac.uk (S.O. El hamali).

http://dx.doi.org/10.1016/j.optlaseng.2015.12.010

solution processing [18]. Radio frequency magnetron sputtering is the most commonly used approach owing to its potential for low temperature growths, industrial applicability, as well as relatively good uniformity and reproducibility [12]. Unfortunately, to produce AZO films with high quality electro-optical characteristics for large area applications, it is typical to require high thermal budget at deposition [19], or at post-deposition processing [20]. At the same time, for further optoelectronic developments there has been an increasing interest in low thermal budget fabrication of metal oxides in order to maintain the characteristics of any underlying layers or the substrate itself, as well as to reduce the long processing times needed for conventional thermal processing. Hence, Excimer Laser Annealing (ELA) has been explored as an ultra-rapid, and spatially localised both in area and depth processing method to realise high quality metal oxide thin films at minimal substrate heating [16,21]. Only a few previously reported studies have explored the effect of ELA on AZO. R. Boukhicha et al. [22] and E. Johnson et al. [23] have reported dramatically improved AZO optical properties via ELA (XeCl 308 nm) and a chemical etching process, but only a moderate resistivity reduction was reported from 1.1×10^{-3} to 0.7×10^{-3} Ω.cm for 1 μm thick AZO samples. Q. Xu et al. [24] have reported a resistivity reduction from 3.4×10^{-3} to 2.2×10^{-3} Ω.cm via processing 200 nm thick AZO films with a cw Nd:YAG laser at 1064 nm. W.-T. Hsiao et al. [25,26] have noticeably reduced the resistivity of 200 nm thick AZO samples after annealing with a cw diode laser at 808 nm, from 4.00×10^{-2} to 2.75×10^{-2} Ω.cm. However, the achieved resistivity values by both Q. Xu et al. and W.-T. Hsiao et al. are too high for use as a practical transparent electrode. Nian et al. [15] combined room temperature pulsed laser deposition and ELA (KrF 248 nm) resulting in highly conductive ($\rho=2.23\times10^{-4}$ Ω.cm) and transparent (85% in the visible range) 250 nm thick AZO films, but a 50 nm i-ZnO was required as a buffer layer.

In the present work we report a complete study of RF magnetron sputter deposited AZO films at different deposition parameters on UV grade fused silica substrates, followed by ELA with a Krypton Fluoride laser (KrF) and with variable number of pulses and laser energy density. Unlike all previously published studies, the deposition and processing conditions concluded in this work offer highly transparent and highly conductive AZO thin films, produced at low thermal budget and with scalable techniques.

2. Experimental procedure

2.1. AZO thin films deposition

Three series of AZO samples, all 180 nm thick, were fabricated using an in-house built RF magnetron sputtering system for deposition at room temperature, where one parameter was changed in each series: (a) with various oxygen concentrations diluted in argon (0–0.5%), (b) with varying RF power (40–240 W) applied to the target, and (c) with varying sputtering pressure (1.5–5.0 mTorr). The UV grade fused silica glass substrates (5 cm × 5 cm) were first cleaned with Decon 90 surfactant solution in water (4% by volume) to remove any dust particles from the substrate surface, followed by sequential ultrasonic cleaning in acetone, methanol, and de-ionised water (for 10 min each). Finally, the substrates were individually demoisturised with high purity dry nitrogen. A three-inch diameter ceramic target of ZnO–Al_2O_3 (98–2 wt%) from Testbourne Ltd. was used. Prior to the deposition, a base pressure of 10^{-5} Pa was achieved in the sputtering chamber. Then, the investigated gas mixture was introduced via two mass flow controllers to produce a sputtering gas of a percentage of oxygen in argon. Pre-sputtering was always performed, with the substrate covered for 10 min at the same parameters as for the subsequent deposition. The substrate to target distance was maintained at 10 cm for all depositions in a sputter-up geometry. The substrate temperature during the deposition was monitored with temperature sensitive labels attached to the back side of the substrate. The substrate was rotated at 8 rpm to provide highly uniform films. The film thickness was monitored by an in-situ interferometric monitor and was cross-checked via Veeco Dektak 6M Stylus Profilometer measurements.

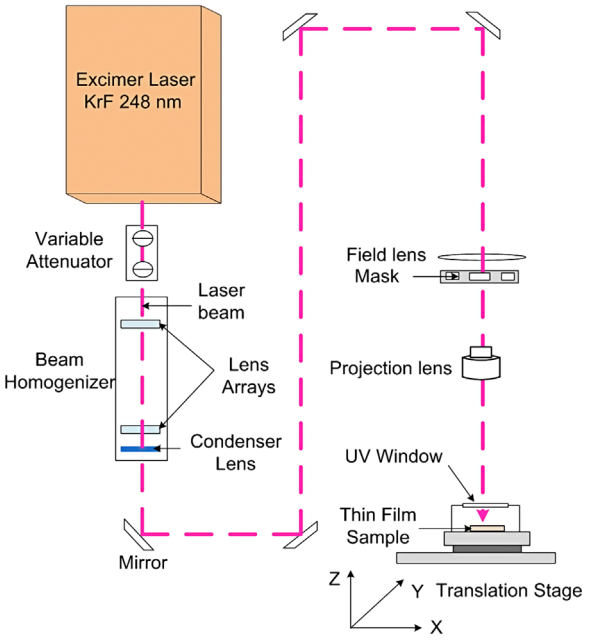

Fig. 1. Schematic diagram of the Excimer Laser Annealing system.

2.2. Excimer laser annealing

ELA was conducted in air at room temperature using the system illustrated in Fig. 1, comprising three main components: (1) the laser source, a Krypton Fluoride (KrF) excimer laser (Lambda Physik LPX 305i), which emits unpolarised light pulses at $\lambda=248$ nm and with a pulse duration of 25 ns. (2) The laser beam delivery and shaping system including an attenuator, a beam homogeniser (Exitech Ltd., type EX-HS-700D, providing laser spots with uniformity better than 2%), mirrors, a field lens, a mask stage, and a projection lens with 1:1 magnification. The laser spot defined by the optics was a square area of 1 cm × 1 cm. (3) An *XYZ* moving stage for samples mounting and manipulation during processing.

Initially, single pulse investigations were conducted in order to identify the threshold energy density required for the onset of an effect on the AZO characteristics, as well as the limit above which material ablation occurs. The investigated energy density range was from 25 to 500 mJ/cm^2 ± 2%, in steps of 25 mJ/cm^2. Clear enhancements in the AZO conductivity and transparency were observed when processed at laser energy densities ≥ 50 mJ/cm^2, while a visible ablation was observed at energy densities ≥ 150 mJ/cm^2. Following the identification of this energy density processing window further investigations were conducted with different number of pulses up to 100.

2.3. AZO thin films characterisation

The essential requirements for TCO applications are low electrical resistivity and high optical transmittance. Thus, this study is focused on these characteristics pre and post ELA application. The

electrical properties including resistivity, mobility, and carrier density for AZO films were evaluated via a Phystech RH2035 Hall measurement system at room temperature, operating in Van der Pauw (VDP) and Hall Effect configuration with a magnetic field of 0.54 T, as well as via a four-point probe resistivity system (4PP). Results presented are the mean average from three measurements for each sample. Optical transmission and reflection spectra were recorded using the Ocean Optics SpectraSuite Software, with a UV/VIS (Ocean Optics USB4000) spectrometer and a NIR (Ocean Optics NIR 256-2.5) spectrometer, and a deuterium–halogen light source (Ocean Optics DH-2000). Surface morphology for the optimised as-deposited and laser annealed AZO samples was characterised by atomic force microscopy AFM using a Veeco Dimension 3100 Scanning Probe Microscope with Nanoscope IV controller, and by scanning electron microscopy SEM with a Hitachi SU-70 Scanning Electron Microscope system operated at 3 kV accelerating voltage, and 300k magnification. Four areas for each sample were examined and a good consistency across the samples was observed. X-ray photoelectron spectroscopy (XPS) was also performed on the optimised as-deposited and ELA-treated AZO samples in an Axis Ultra DLD system by Kratos with an aluminium anode (Al Kα 1486.6 eV).

3. Results and discussion

The sample series with varying oxygen ratio during the deposition showed that 0.2% of oxygen in argon is needed to achieve an adequate long-term replenishment of oxygen on the target surface and thus provide reproducible electrical and optical characteristics for the AZO films. This is due to the fact that oxygen and zinc have different sputtering probabilities, and sputtering in pure argon for a long period is likely to result in oxygen deficiency on the target surface [12]. Hence, the series of samples with varying RF power as well as those with varying sputtering pressure were deposited at 0.2% of oxygen in argon. Whilst there was no intentional heating applied to the substrate, the substrate temperature increased with the applied RF power reaching a maximum of 53 °C at 240 W, as shown in Fig. 2.

3.1. Electrical properties

The study of the electrical properties of AZO revealed that they are profoundly governed by the deposition parameters. The resistivity measurements via both 4PP and VDP techniques are very consistent. Fig. 3 (dashed lines) demonstrated that as the RF power is increased, both the density and the Hall mobility of the free electrons are increased, and thus the electrical resistivity is decreased. These findings are in line with previous studies [13,27], and can be explained as follows: (1) with increasing the applied RF power, the kinetic energy of the sputtered atoms and thus their surface mobility across the substrate are increased. These atoms will therefore organise themselves in a better crystal structure with less electron trapping and scattering defects, which leads eventually to increasing the free carrier density and mobility [12,13,27]. (2) The free carrier density increase could also be attributed to the increased energy of the sputtered species and the thermalisation effect of the glow discharge with RF power, which is confirmed by the temperature labels. Consequently, the activation of Al atoms into zinc oxide might be enhanced [27]. However, both mechanisms described above for decreasing the resistivity with increasing the RF power reach a plateau at 180 W, beyond which only a marginal further improvement is observed. Taking into account the growth rate levelling off and the unintentional substrate heating increase at higher RF powers, we consider the 180 W to be the optimum RF power for high quality AZO depositions at low temperature in this work.

Both the RF power and sputtering pressure are directly linked to the energy of the sputtered atoms and have opposite impacts on the deposited film's characteristics. Fig. 4 illustrates that increasing the sputtering pressure significantly increases the AZO resistivity

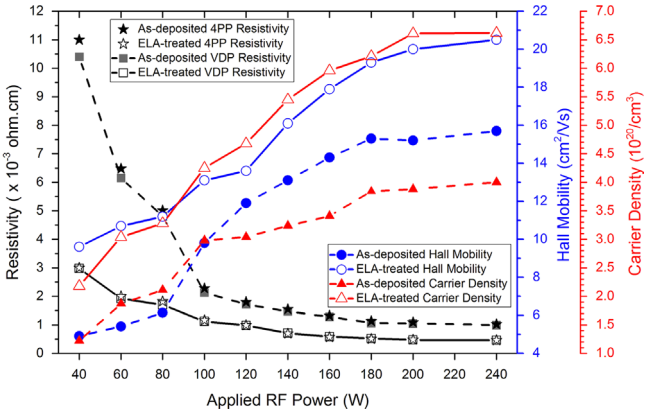

Fig. 3. Resistivity, Hall mobility, and carrier density as a function of the applied RF power for the as-deposited AZO films (2.0 mTorr of 0.2% O_2 in Ar, dashed lines), and after ELA (with 5 pulses at 125 mJ/cm^2, solid lines).

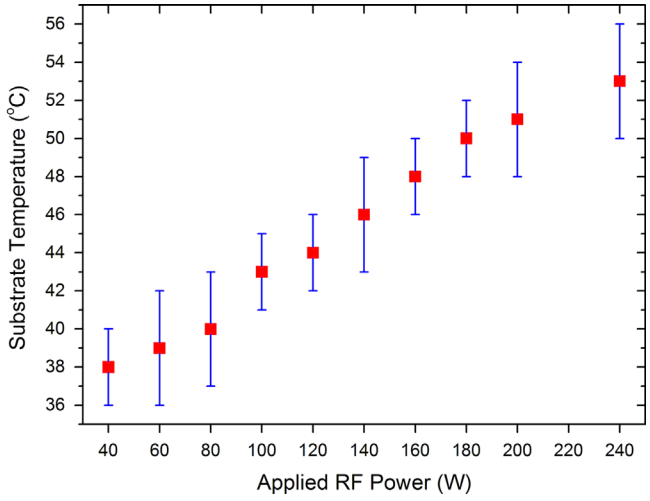

Fig. 2. The substrate temperature (not intentionally heated) as a function of the applied RF power.

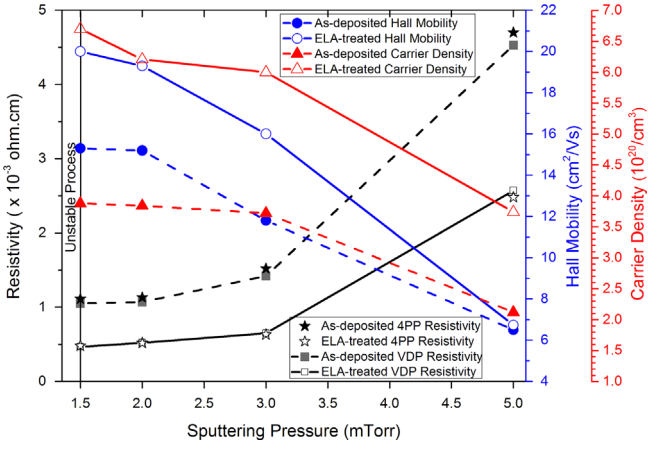

Fig. 4. Resistivity, Hall mobility, and carrier density as a function of the sputtering pressure for the as-deposited AZO films (180 W, and 0.2% O_2 in Ar, dashed lines), and after ELA (with 5 pulses at 125 mJ/cm^2, solid lines).

as a result of reducing the free carriers' mobility and density (dashed lines in Fig. 4). The effect of the sputtering pressure on the resistivity of AZO is attributed to decreasing the mean free path of the sputtered species due to increasing the collisions between the sputtered atoms and the residual gas ions at higher pressure. Consequently, the sputtered species will lose energy and thus their surface mobility on the substrate is reduced, resulting in degrading the film doping efficiency, compactness, and crystallinity due to microstructural defects such as oxygen species diffused into grain boundaries. This would result in electron trapping from the conduction band, increasing the free electron scattering, and therefore reducing the free carrier density and mobility [17,27,28]. It should be noted that utilising sputtering pressures lower than 1.5 mTorr was not possible due to difficulties in maintaining the plasma in the sputtering chamber; probably due to inadequate quantity of sputtering gasses. Even at 1.5 mTorr the sputtering process was found to be intermittently unstable, by means of either the plasma going off or reflected RF power suddenly appearing. Therefore, 2.0 mTorr was chosen as the optimum working pressure in this work.

Regarding the electrical properties of the AZO samples after ELA, Fig. 5 illustrates the effect of different ELA conditions (laser fluences and number of pulses) on the resistivity of AZO samples deposited at different conditions (RF power and sputtering pressure). It was found that ELA even with one pulse reduces the resistivity, with the reduction becoming greater as the laser fluence increased up to 125 mJ/cm^2. Furthermore, when the number of pulses was increased to five at this fluence, the electrical resistivity was reduced for all samples by 50% compared to the as-deposited samples. Increasing the number of pulses above five at 125 mJ/cm^2 either showed no further resistivity decrease or resulted in material ablation and hence resistivity increase. The material ablation is attributed to heat accumulation during ELA with multiple pulses that leads to a temperature higher than that reached by a single pulse and at the same time higher than the AZO melting temperature [15]. Therefore, the optimum ELA processing in this work is considered to be 5 pulses at 125 mJ/cm^2.

Hall Effect measurements revealed that the conductivity improvement upon ELA is a result of the concurrent increase of the free carrier density as well as the Hall mobility (see solid lines in Figs. 3 and 4).

According to the AFM and SEM images as shown in Fig. 6, the application of ELA to AZO results in a just noticeable surface-particle size enlargement, and more uniform and compact thin film surface. Also, AFM images showed that the surface flatness is improved after annealing, the arithmetic roughness Ra is reduced from 1.41 to 1.14 nm after ELA. Surface morphology changes upon ELA could not justify the noticed mobility enhancement from 15.3 to 19.3 cm^2/V s in their own merit. Moreover, Energy Dispersive X-ray Spectroscopy (EDS) showed that all the samples, irrespective of deposition and ELA conditions, showed an unchanged atomic concentration of Al (within experimental error) at 2.12 $\pm$ 0.08 at%. Hence, the noticed free carrier density changes could be attributed to variations in ZnO doping efficiency and trap states density between the samples and in particular after ELA treatment. Oxygen related defects including oxygen vacancies, native point defects, and adsorbed oxygen defects have an important impact on the free carrier density and mobility of ZnO-based films [12,28]. To examine oxygen related defects changes upon ELA, high-resolution XPS measurements were performed on the optimised as-deposited and ELA-treated AZO samples after 60 s etching by Ar^+ ion sputtering (282.0 eV) to remove surface contaminations. To mention, minor differences in the Zn2p and Al2p spectra were observed. The O1s spectra demonstrated more noticeable changes upon ELA treatment. In order to study the oxygen state changes in detail, the O1s spectra were deconvoluted into three Gaussian sub-spectral components positioned at binding energies as shown in Fig. 7. The sub-spectral component O1s (I) at 529.9 eV is attributed to O^{2-} ions on wurtzite ZnO, fully surrounded by Zn^{2+} cations or the substitutional Al^{3+} cations. The second component O1s (II) at 531.2 eV is linked to O^{2-} ions in the oxygen deficient regions within the ZnO matrix. The third component O1s (III) at 531.9 eV is assigned to adsorbed O_2 atoms, or hydroxyl group such as H_2O, or $-CO_3$. These species tend to diffuse into grain boundaries and inter

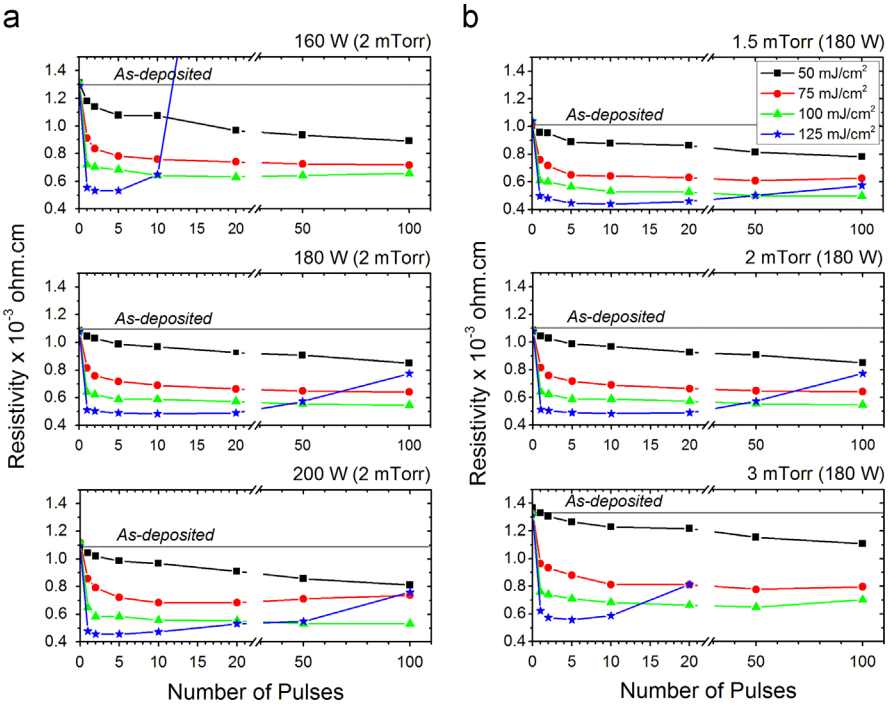

Fig. 5. The effect of ELA at different energy densities and number of pulses on AZO resistivity as a function of (a) the applied RF power, and (b) the sputtering pressure. The resistivity at 0 pulses represents the as-deposited AZO resistivity.

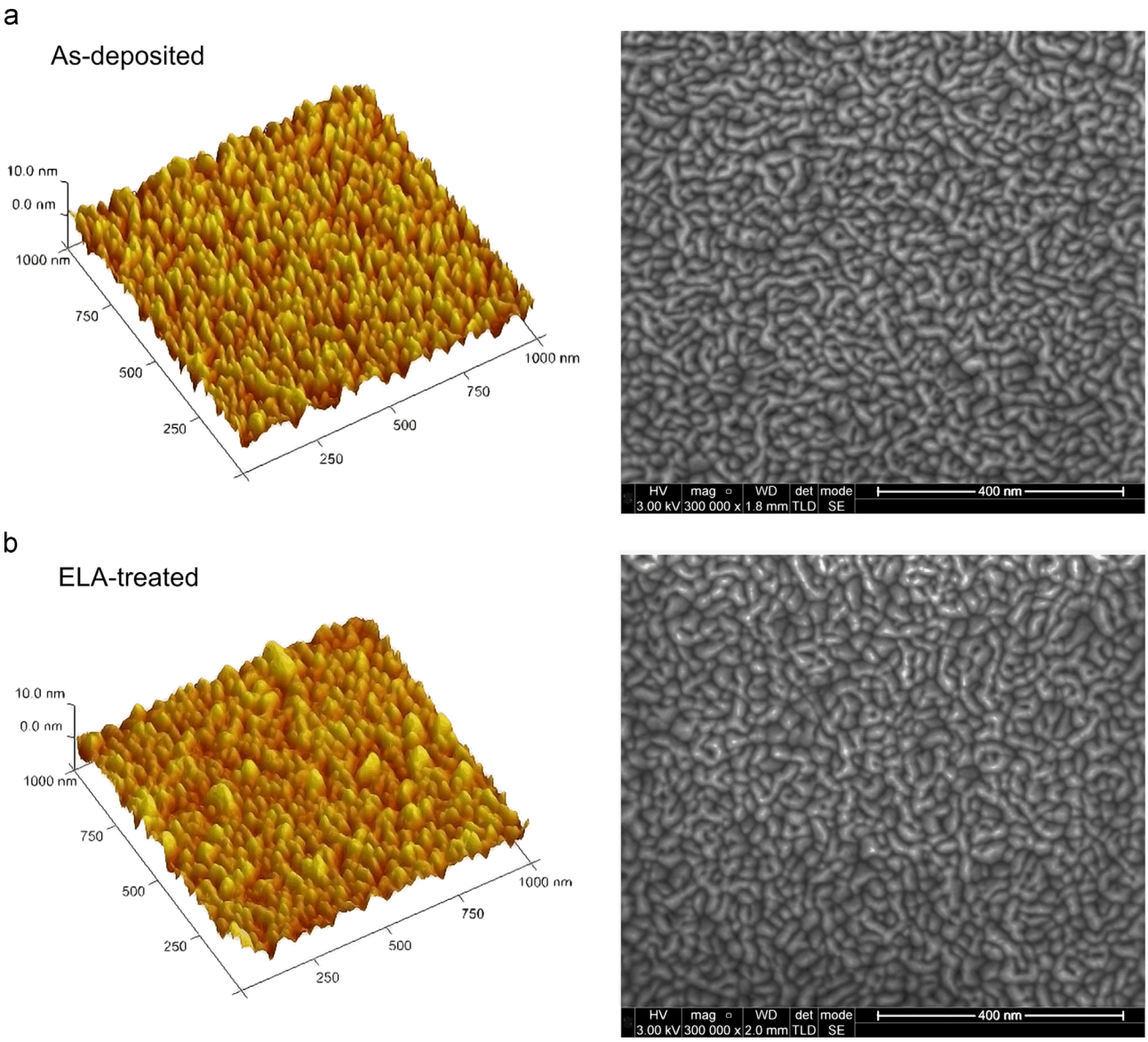

Fig. 6. AFM and SEM images for (a) the optimum as-deposited sample (180 W, 2.0 mTorr), and (b) the optimum ELA-treated sample (5 pulses at 125 mJ/cm^2).

grain voids acting as electron trapping and scattering centres [15,29]. The details of the three components are presented in Table 1. The components area ratio is calculated relative to the overall O1s peak area for each sample. It was revealed that the application of ELA to AZO samples results in an increased O1s (I) component, while the O1s (II) and O1s (III) components are reduced. These results indicate less oxygen vacancies (native point defects) and adsorbed defects i.e. better ZnO crystal structure is achieved upon ELA. The observed reduction of O1s (III) component implies reduced electron trap density at grain boundaries and the resultant barrier height between the grains via ELA. Consequently, the free carrier density and mobility both are enhanced. Similar findings were reported by prior publications [15,18]. In addition, since all the AZO samples were deposited without intentional substrate heating not all Al atoms are initially effectively incorporated into the zinc oxide lattice due to insufficient kinetic energy. The non-activated Al atoms could be agglomerating at non-crystalline regions such as grain boundaries causing carrier-scattering. The ELA treatment would provide the Al atoms with the needed activation energy to replace Zn atoms in the ZnO matrix and contribute to free electrons [11,16,20]. The decrease in oxygen vacancy density observed in XPS measurements could be attributed to Al activation into ZnO lattice upon ELA [17].

According to Seto model [30], the noticed increase in the free carrier density upon annealing would deactivate the trap states at the grain boundaries and reduce the carrier-depleted area on both sides of grain boundaries resulting in decreasing the potential barrier between the grains and thus enhancing the free carrier mobility [28,30].

3.2. Optical properties

All the as-deposited AZO samples showed an average visible transmission around 85% that exhibited a minor reduction as the applied RF power is increased or the sputtering pressure is reduced compared to the optimum conditions (180 W and 2 mTorr), as shown in Figs. 8 and 9. These trends could be attributed to the film roughness increase due to increasing the deposited film bombardments by the sputtered species at high power or low pressure [11]. Upon excimer laser annealing the average visible transmission was enhanced to about 90% for all AZO samples. This improvement can be related to reduce optical

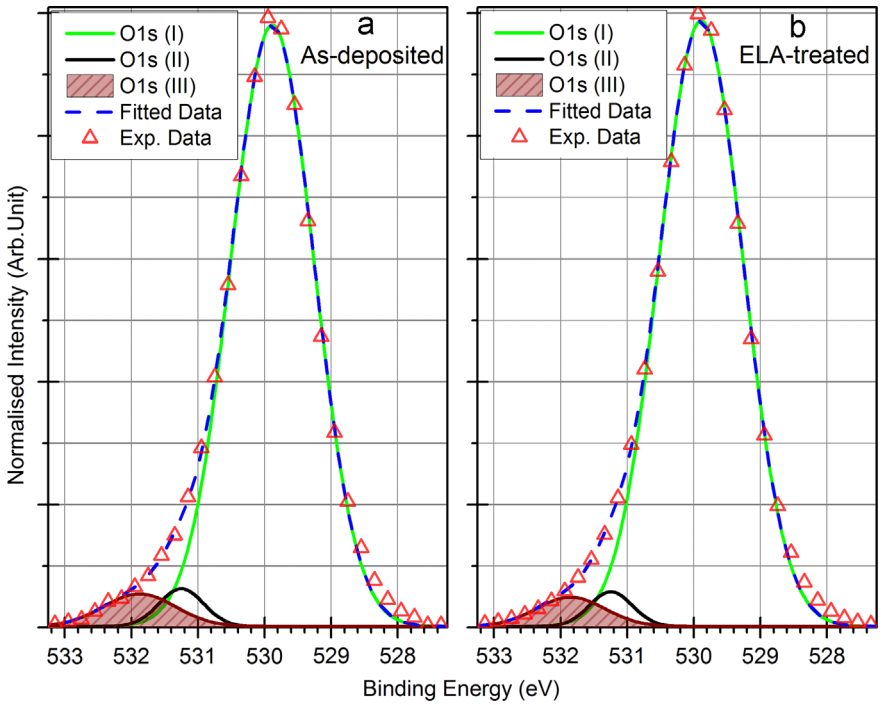

Fig. 7. High resolution O1s XPS spectra for (a) the optimum as-deposited sample, and (b) the optimum ELA-treated sample deconvoluted into three sub-spectral components.

Table 1
Details of the deconvoluted sub-spectral components of the high resolution O1s XPS spectra for the optimum as-deposited and ELA-treated AZO films.

AZO sample	O1s(I)		O1s(II)		O1s(III)	
	Area ratio (%)	FWHM (eV)	Area ratio (%)	FWHM (eV)	Area ratio (%)	FWHM (eV)
As-deposited	91.51	1.47	3.25	0.81	4.52	1.31
ELA-treated	93.41	1.48	2.81	0.77	3.76	1.25

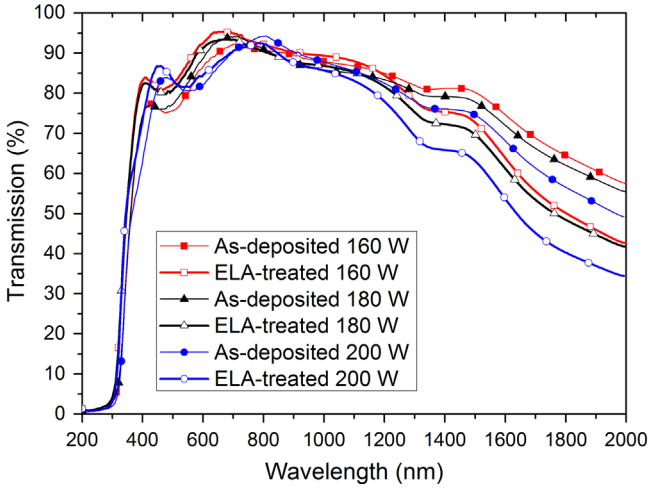

Fig. 8. Optical transmission spectra as a function of the applied RF power for the as-deposited AZO films (at 2.0 mTorr of 0.2% O_2 in Ar, solid data points), and after ELA (5 pulses at 125 mJ/cm^2, hollow data points).

scattering events because of reducing the film roughness and microstructural defects as demonstrated with the presented AFM and XPS data [11,16]. Moreover, the absorption edge was blue

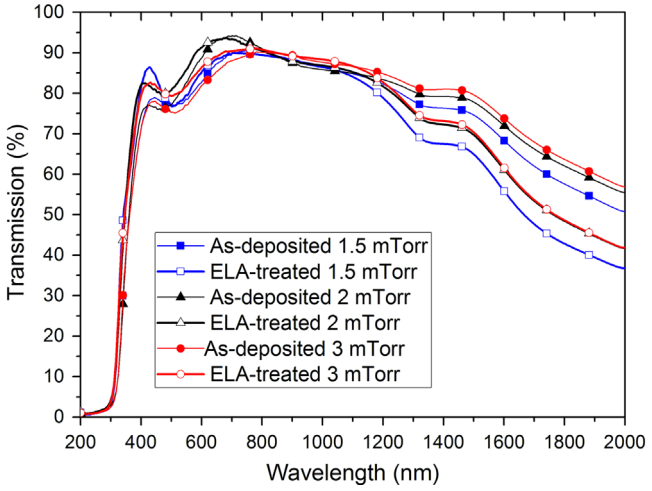

Fig. 9. Optical transmission spectra as a function of the sputtering pressure for the as-deposited AZO films (at 180 W, and 0.2% O_2 in Ar, solid data points), and after ELA (5 pulses at 125 mJ/cm^2, hollow data points).

shifted, as shown in Fig. 10, owing to the carrier density increase upon annealing, resulting in the bandgap widening according to the Burstein–Moss model [31]. The bandgap (E_g) for the optimum as-deposited AZO sample (180 W, 2 mTorr) was estimated by Tauc et al. model [32] and found to increase after ELA (5 pulses at 125 mJ/cm^2), from 3.69 to 3.80 eV, as illustrated in the inset graph of Fig. 10. At longer wavelengths (infrared region $\lambda > 1000$ nm), however, the transmission spectra demonstrated a decrease that corresponds to the free carrier density increase when AZO films deposited at higher RF power, lower pressure, or after ELA due to increasing the free carrier reflection at higher carrier density leading to shifting the plasma frequency towards shorter wavelengths [31,33].

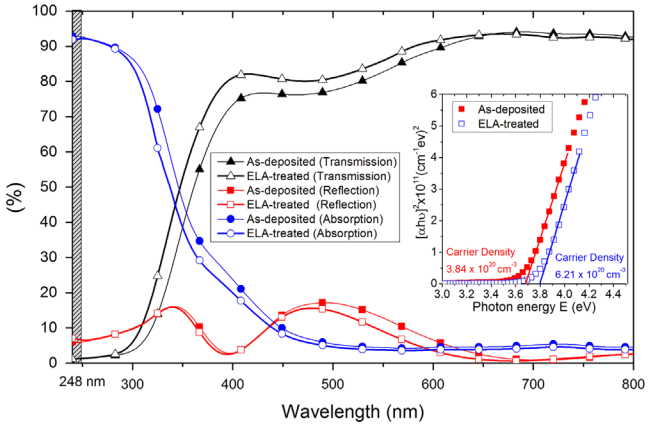

Fig. 10. Transmission, reflection, and absorption UV/VIS spectra of the optimum as-deposited and the optimum ELA-treated AZO thin films. The inset graph shows linear extrapolations of Tauc's plot for these samples. (For interpretation of the references to color in this figure, the reader is referred to the web version of this article.)

4. Conclusion

In this work, the potential for nanosecond ELA to significantly enhance the electrical and optical characteristics of AZO films deposited by RF-magnetron sputtering at no intentional substrate heating has been demonstrated. A broad range of parameters for sputter-deposition and ELA process has been explored. Under the optimised deposition parameters, 180 nm thick AZO thin films showed a resistivity of 1×10^{-3} Ω.cm, corresponding to a sheet resistance of 56 Ω/sq, with a Hall mobility 15.3 cm^2/V s, and a carrier density 3.84×10^{20} cm^{-3}. These electrical characteristics were noticeably enhanced after ELA with the optimised conditions of 5 pulses at 125 mJ/cm^2 to a resistivity of 5×10^{-4} Ω.cm, corresponding to a sheet resistance of 28 Ω/sq, with a Hall mobility 19.3 cm^2/V s, and a carrier density 6.21×10^{20} cm^{-3}. Moreover, the average visible transparency was enhanced from 85% to 90%, and the bandgap was enlarged from 3.69 to 3.80 eV. This combination of RF magnetron sputtering and ELA produces reliably AZO thin films with electro-optical characteristics that are very close to those of ITO, but crucially via low thermal-budget processing. The adapted fabrication route could be applied to large volume production, as the needed energy density for optimum ELA to half the resistivity is rather low (125 mJ/cm^2).

Acknowledgement

The authors would like to acknowledge the Ministry of Higher Education and Scientific Research-Libya for funding the Ph.D. programme of co-author S.O. El hamali (grant 700/2007EX692/2012).

References

[1] Liu H, Avrutin V, Izyumskaya N, Özgür Ü, Morkoç H. Transparent conducting oxides for electrode applications in light emitting and absorbing devices. Superlattices Microstruct 2010;48:458–84.
[2] Minami T. Transparent conducting oxide semiconductors for transparent electrodes. Semicond Sci Technol 2005;20:S35–44.
[3] Ellmer K. Past achievements and future challenges in the development of optically transparent electrodes. Nat Photon- 2010;6:809–17.
[4] Minami T. Present status of transparent conducting oxide thin-film development for Indium-Tin-Oxide (ITO) substitutes. Thin Solid Films 2008;516:5822–8.
[5] Cairns DR, Witte II RP, Sparacin DK, Sachsman SM, Paine DC, Crawford GP, Newton R. Strain-dependent electrical resistance of tin-doped indium oxide on polymer substrates. Appl Phys Lett 2000;76:1425–7.
[6] Mohanta A, Thareja RK. Temperature-dependent S-shaped photoluminescence in ZnCdO alloy. J Appl Phys 2010;107:084904-1–4.
[7] Narayan J, Sharma AK, Kvit A, Jin C, Muth J, Holland O. Novel cubic $Zn_xMg_{1-x}O$ epitaxial heterostructures on Si (100) substrates. Solid State Commun 2001;121:9–13.
[8] Janotti A, Van de Walle, Chris G. Fundamentals of zinc oxide as a semiconductor. Rep Prog Phys 2009;72:126501–29.
[9] Gong SC, Choi Y, Kim H, Park C, Park H, Jang JG, Chang HJ, Yeom GY. Aluminum-doped zinc oxide formed by atomic layer deposition for use as anodes in organic light emitting diodes. J Vac Sci Technol A 2013;31 01A101-5.
[10] Oh B, Jeong M, Moon T, Lee W, Myoung J, Hwang J, Seo D. Transparent conductive Al-doped ZnO films for liquid crystal displays. J Appl Phys 2006;99:124505-1–4.
[11] Kim KH, Park KC, Ma DY. Structural, electrical and optical properties of aluminum doped zinc oxide films prepared by radio frequency magnetron sputtering. J Appl Phys 1997;81:7764–72.
[12] Ellmer K. Magnetron sputtering of transparent conductive zinc oxide: relation between the sputtering parameters and the electronic properties. J Phys D 2000;33:R17–32.
[13] Prabhakar T, Dai L, Zhang L, Yang R, Li L, Guo T, Yan Y. Effects of growth process on the optical and electrical properties in Al-doped ZnO thin films. J Appl Phys 2014;115:083702-1–7.
[14] Zhang MY, Nian Q, Cheng GJ. Room temperature deposition of alumina-doped zinc oxide on flexible substrates by direct pulsed laser recrystallization. Appl Phys Lett 2012;100:151902-1–4.
[15] Nian Q, Zhang MY, Schwartz BD, Cheng GJ. Ultraviolet laser crystallized ZnO:Al films on sapphire with high Hall mobility for simultaneous enhancement of conductivity and transparency. Appl Phys Lett 2014;104:201907-1–5.
[16] Tsang WM, Wong FL, Fung MK, Chang J, Lee CS, Lee ST. Transparent conducting aluminum-doped zinc oxide thin film prepared by sol–gel process followed by laser irradiation treatment. Thin Solid Films 2008;517:891–5.
[17] Mohanta A, Simmons JG, Everitt HO, Shen G, Kim SM, Kung P. Effect of pressure and Al doping on structural and optical properties of ZnO nanowires synthesized by chemical vapor deposition. J Lumin 2014;146:470–4.
[18] Hagendorfer H, Lienau K, Nishiwaki S, Fella CM, Kranz L, Uhl AR, Jaeger D, Luo L, Gretener C, Buecheler S, Romanyuk YE, Tiwari AN. Highly transparent and conductive ZnO:Al thin films from a low temperature aqueous solution approach. Adv Mater 2014;26:632–6.
[19] Minami T, Sato H, Imamoto H, Takata. S. Substrate temperature dependence of transparent conducting Al-doped ZnO thin films prepared by magnetron sputtering. Jpn J Appl Phys 1992;31:L257–61.
[20] Ruske F, Roczen M, Lee K, Wimmer M, Gall S, Hüpkes J, Hrunski D, Rech B. Improved electrical transport in Al-doped zinc oxide by thermal treatment. J Appl Phys 2010;107:013708-1–8.
[21] Cranton WM, Wilson SL, Ranson R, Koutsogeorgis DC, Chi K, Hedgley R, Scott J, Lipiec S, Spiller A, Speakman S. Excimer laser processing of inkjet-printed and sputter-deposited transparent conducting SnO_2:Sb for flexible electronics. Thin Solid Films 2007;515:8534–8.
[22] Boukhicha R, Charpentier C, Prod'Homme P, Cabarrocas PR i, Lerat J, Emeraud T, Johnson E. Influence of sputtering conditions on the optical and electrical properties of laser annealed and wet etched room temperature sputtered ZnO:Al. Thin Solid Films, 555; 2014. p. 13–7.
[23] Johnson E, Prod'homme P, Boniface C, Huet K, Emeraud T, Cabarrocas PR i. Excimer laser annealing and chemical texturing of ZnO:Al sputtered at room temperature for photovoltaic applications. Sol Energy Mater Sol Cells, 95; 2011. p. 2823–30.
[24] Xu Q, Hong R, Huang H, Zhang Z, Zhang M, Chen X, Wu. ZY. Laser annealing effect on optical and electrical properties of Al doped ZnO films. Opt Laser Technol 2013;45:513–7.
[25] Hsiao W, Tseng S, Chung C, Chiang D, Huang K, Lin K, Li L, Chen M. Effect on structural, optical and electrical properties of aluminum-doped zinc oxide films using diode laser annealing. Opt Laser Technol 2015;68:41–7.
[26] Hsiao W, Tseng S, Huang K, Chiang D. Electrode patterning and annealing processes of aluminum-doped zinc oxide thin films using a UV laser system. Opt Lasers Eng 2013;51:15–22.
[27] Rahmane S, Djouadi M, Aida M, Barreau N, Abdallah B, Hadj Zoubir. N. Power and pressure effects upon magnetron sputtered aluminum doped ZnO films properties. Thin Solid Films 2010;519:5–10.
[28] Ellmer K. Resistivity of polycrystalline zinc oxide films: current status and physical limit. J Phys D 2001;34:3097–108.
[29] Chen M, Wang X, Yu Y, Pei Z, Bai X, Sun C, Huang R, Wen L. X-ray photoelectron spectroscopy and auger electron spectroscopy studies of Al-doped ZnO films. Appl Surf Sci 2000;158:134–40.
[30] Seto. JY. The electrical properties of polycrystalline silicon films. J Appl Phys 1975;46:5247–54.
[31] Burstein E. Anomalous optical absorption limit in InSb. Phys Rev B 1954;93:632–3.
[32] Tauc J, Grigorovici R, Vancu A. Optical properties and electronic structure of amorphous germanium. Phys Status Solidi (B) 1966;15:627–37.
[33] Dimova-Malinovska D, Tzenov N, Tzolov M, Vassilev L. Optical and electrical properties of R.F. magnetron sputtered ZnO:Al thin films. Mater Sci Eng: B, 52; 1998. p. 59–62.